# Supporting Information

## Programmable Folding Kinetics in Single-Composition Hydrogel Actuators via UV-Induced Microphase Separation

Gi-Yeon Han,†[a] Yumi Rho,†[b] Jiayu Zhao,[b] Willie Lei,[b] Jinhye Bae*[a,b]

Gi-Yeon Han, Jinhye Bae

[a] Department of Chemical Engineering, Chung-Ang University, Seoul, 06974, Republic of Korea

Yumi Rho, Jiayu Zhao, Willie Lei, Jinhye Bae

[b] Department of Chemical and Nano Engineering, University of California San Diego, La Jolla, CA 92093, USA

† These authors contributed equally to this work

Corresponding author E-mail: j3bae@ucsd.edu, jbae@cau.ac.kr

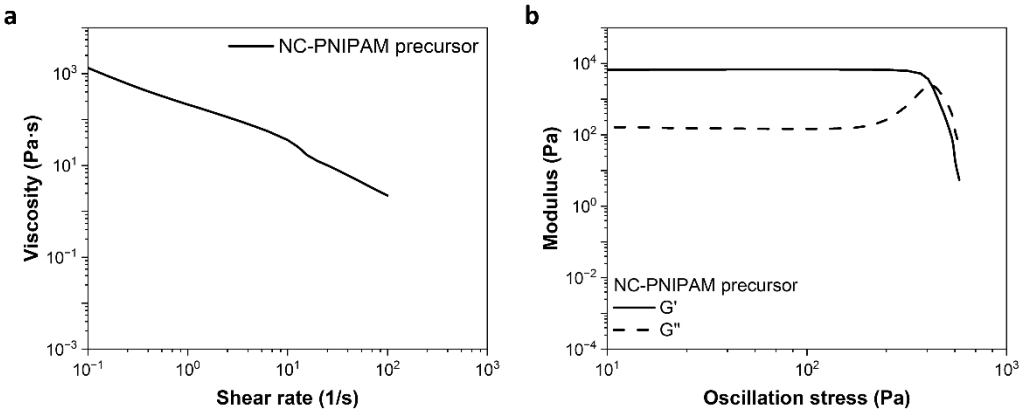


**Fig. S1.** Rheological properties of the NC-PNIPAM precursor. a) Measured viscosity under shear rate sweep mode at steady state. b) Measured modulus under strain sweep mode at oscillatory state.

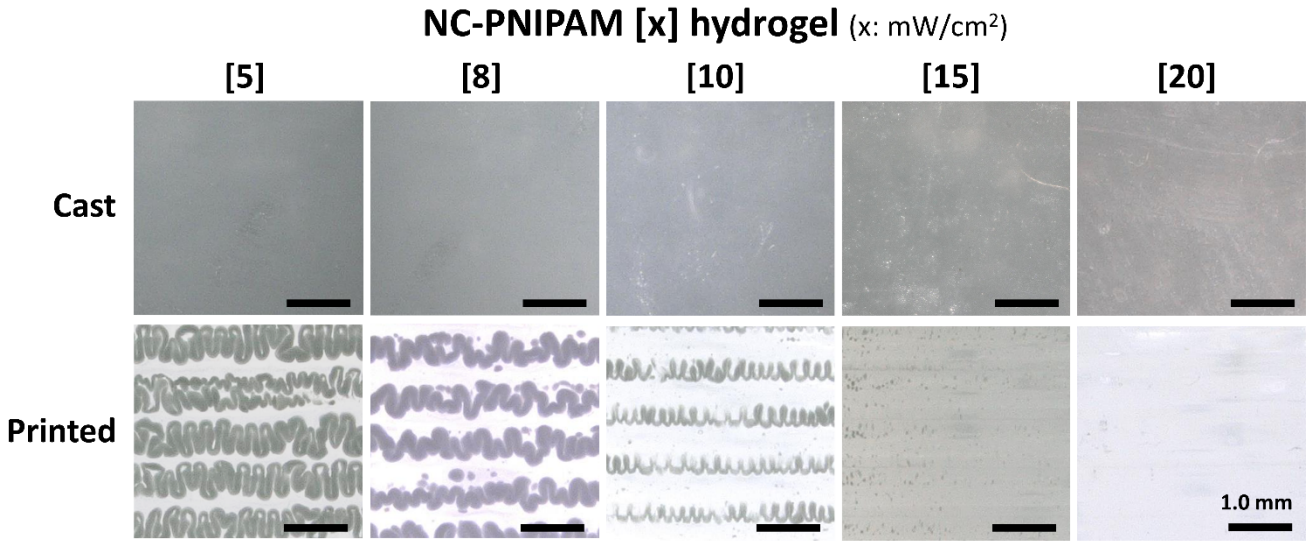


**Fig. S2.** Optical micrographs of the cast and extrusion-printed NC-PNIPAM [x] (x: 5, 8, 10, 15, and 20) hydrogels.

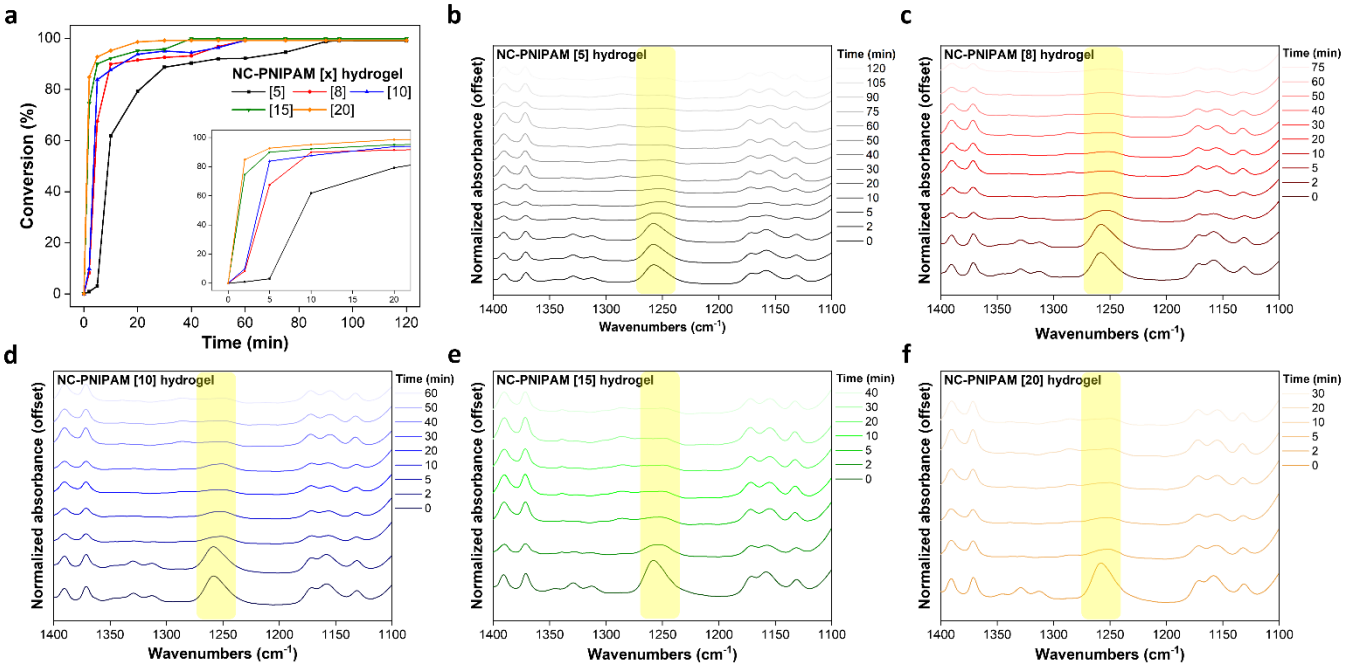


**Fig. S3.** a) Conversion of the NC-PNIPAM precursor under 365 nm UV light irradiation at different time points. Conversion of the NC-PNIPAM precursor was calculated by reduction rate of 1,270 $cm^{-1}$ band (acrylate C=C) at the FT-IR spectra. b, c, d, e, and f) Change of the FT-IR spectra of the NC-PNIPAM precursor with different UV intensities and irradiation time.

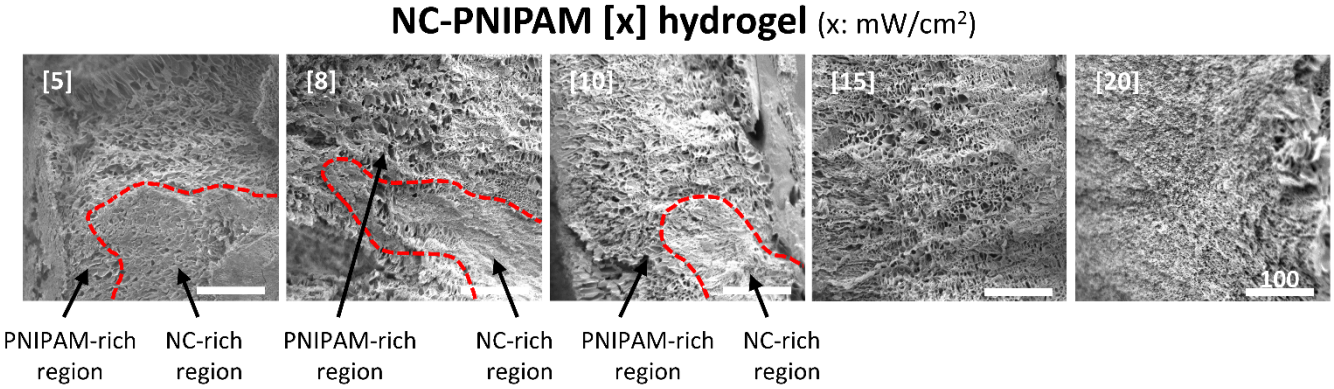


**Fig. S4.** SEM images of the freeze-dried NC-PNIPAM [x] (x:5, 8, 10, 15, and 20) hydrogels (magnification: 500X). The red dashed lines in the NC-PNIPAM [x] (x: 5, 8, and 10) hydrogels represent the boundaries between the NIPAM-rich and NC-rich regions. NC-PNIPAM [x] (x: 15 and 20) hydrogels exhibit no observable NC-rich region.

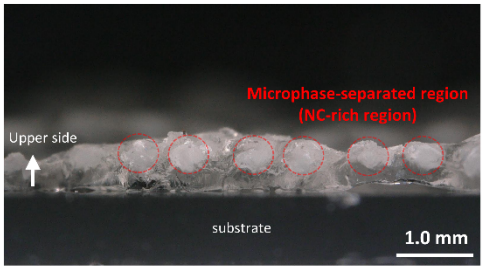


**Fig. S5.** Side view image of NC-PNIPAM [8] hydrogel. Red dotted circles represent the microphase-separated (NC-rich) regions.

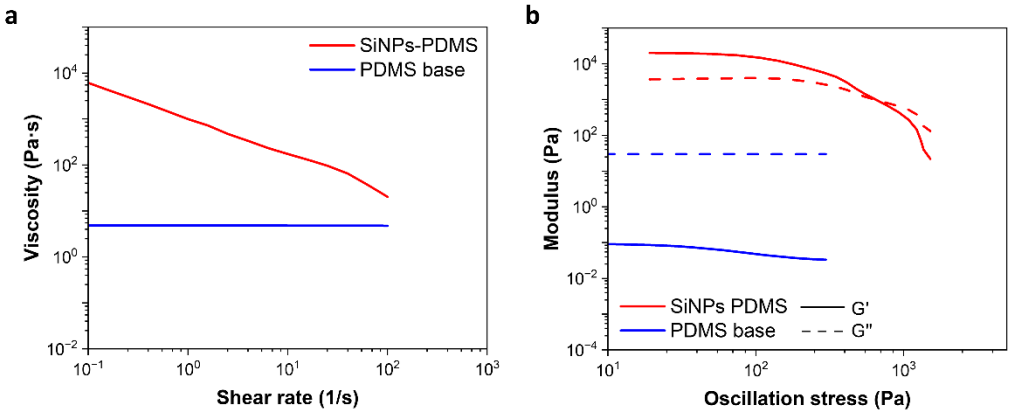


**Fig. S6.** Rheological properties of the pure PDMS base and SiNPs-PDMS resin. a) Measured viscosity under shear rate sweep mode at steady state. b) Measured modulus under strain sweep mode at oscillatory state.

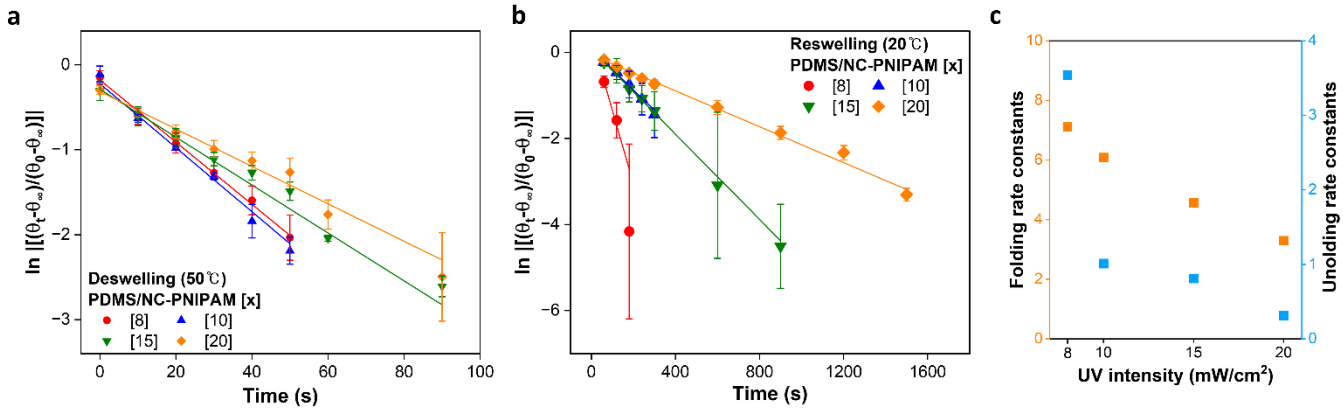


**Fig. S7**. The relative change of a) folding and b)unfolding angle ( $\ln\left|\frac{\theta_t-\theta_\infty}{\theta_0-\theta_\infty}\right|$ ) of PDMS/NC-PNIPAM [x] (x: 8, 10, 15, and 20) and fitted curve as a function of time, where $\theta_0$, $\theta_t$, and $\theta_\infty$ are folding-unfolding angle of hinge at initial, time t, and quilibrium states, respectively. c) Calculated folding-unfolding rate constants of PDMS/NC-PNIPAM [x] (x: 8, 10, 15, and 20). The folding-unfolding rate constants was calculated by dividing the equilibrium folding-unfolding angle by the folding-unfolding equilibrium time (inverse of the slope of the fitted curve).

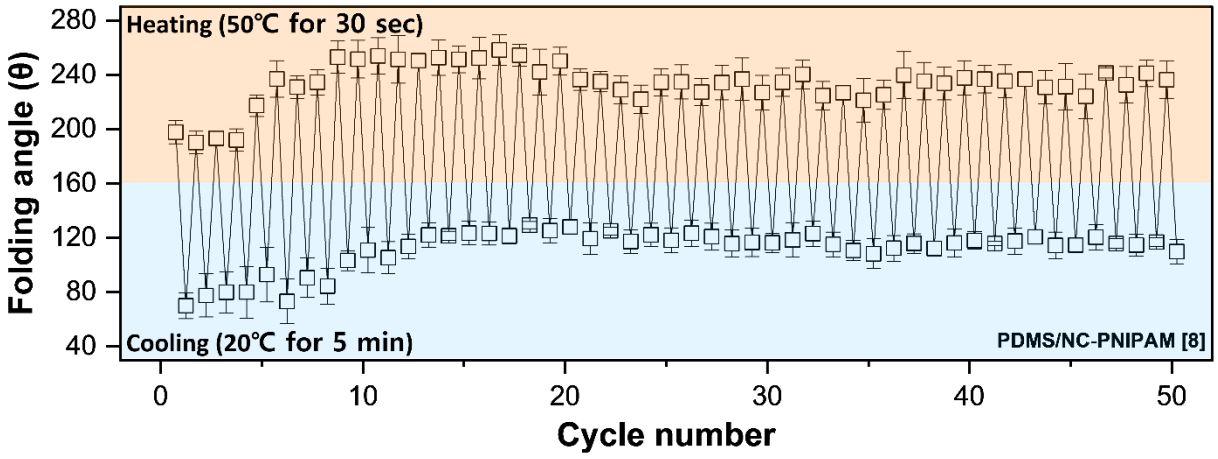


**Fig. S8**. Reversible folding angle change of the PDMS/NC-PNIPAM [8] under 50 consecutive cycles of deswelling (50℃ DIW for 30 seconds) and reswelling (20℃ DIW for 5 minutes). The cyclic test was conducted without rest.

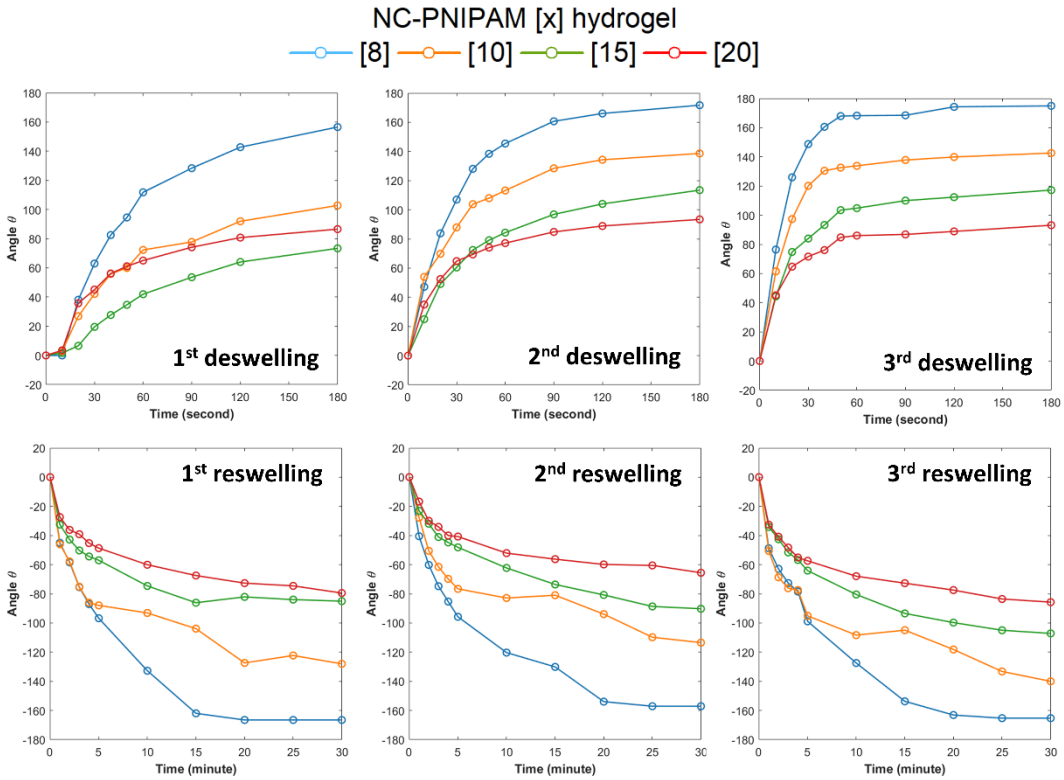


**Fig. S9.** Angular change in the hinge units, which consisting of NC-PNIPAM [x] (x = 8, 10, 15 and 20) hydrogels, of the 4-hinge strip when immersed in 50°C (deswelling) and 20°C (reswelling) DIW, respectively.

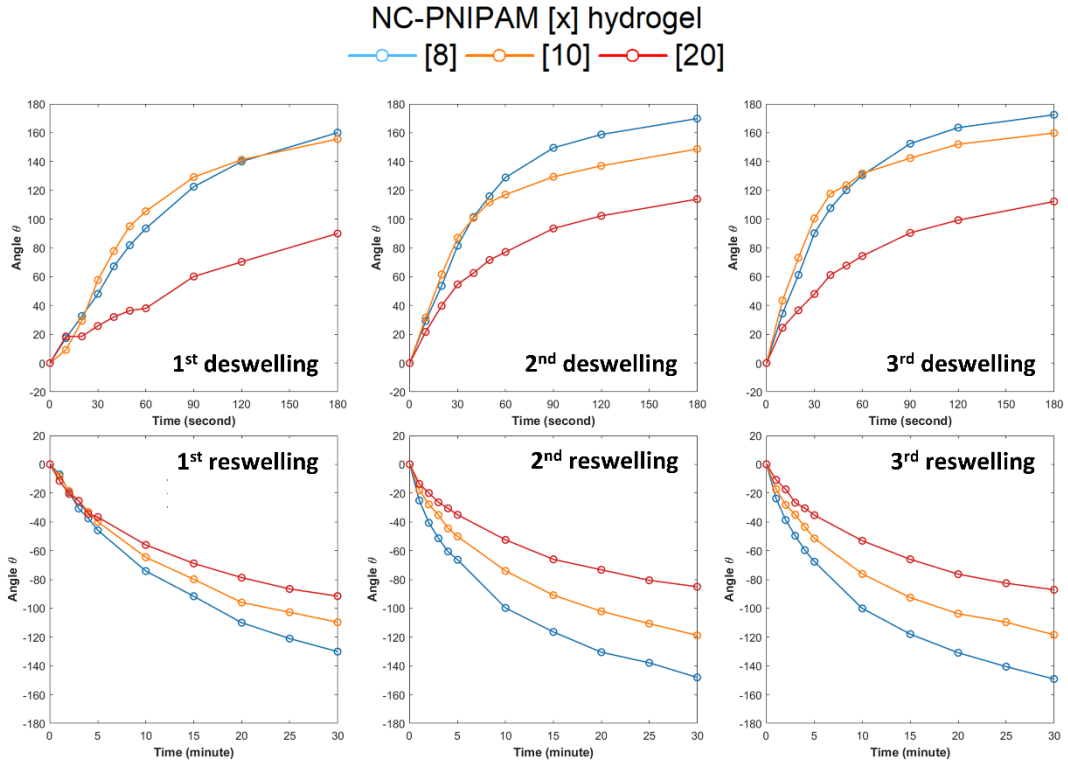


**Fig. S10.** Angular change in the hinge units, which consist of NC-PNIPAM [x] (x = 8, 10, and 20) hydrogels, of the 3-hinge gripper when immersed in 50°C (deswelling) and 20°C (reswelling) DIW, respectively.

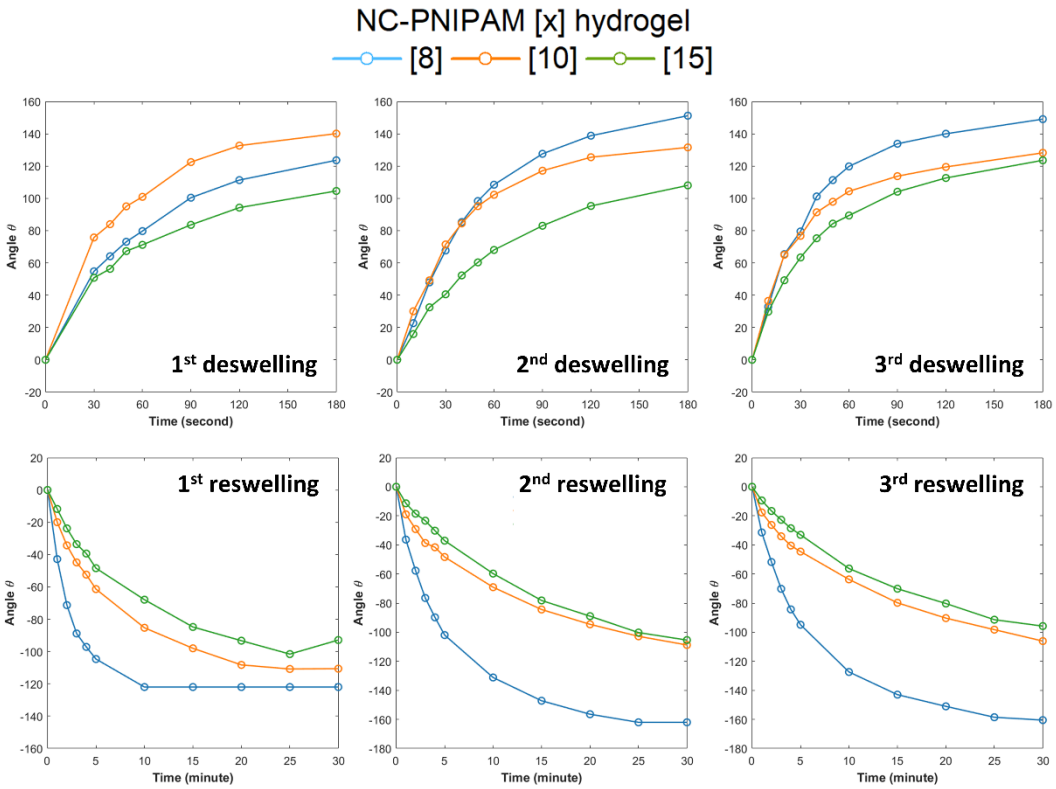


**Fig. S11.** Angular change in the hinge units, which consist of NC-PNIPAM [x] (x = 8, 10, and 15) hydrogels, of the 3-hinge gripper when immersed in 50°C (deswelling) and 20°C (reswelling) DIW, respectively.

**Table S1.** Values derived from the folding-unfolding kinetics equation. The equation is $\ln\left|\frac{\theta_t-\theta_\infty}{\theta_0-\theta_\infty}\right| = -\frac{t}{\tau} + \ln A$, where $\theta_0$, $\theta_t$, and $\theta_\infty$ are folding angle of hinge at initial, time t, and quilibrium states, respectively. τ stands for the equilibrium time, and A is an intercept.

| PDMS/NC PNIPAM [x] | x | Equilibrium time (τ) (sec) | Intercept ($\ln A$) | $R^2$ | Equilibrium folding-unfolding angle (eq°) | Folding-unfolding rate constants (eq°/τ) |
|---|---|---|---|---|---|---|
| Deswelling (folding) | 8 | 27.3 | -0.17752 | 0.995 | 194.03 | 7.11 |
| | 10 | 26.5 | -0.22139 | 0.981 | 161.22 | 6.08 |
| | 15 | 35.4 | -0.28717 | 0.975 | 161.69 | 4.56 |
| | 20 | 45.4 | -0.31388 | 0.984 | 149.26 | 3.29 |
| Reswelling (unfolding) | 8 | 58.7 | 0.34768 | 0.916 | 207.88 | 3.54 |
| | 10 | 211.4 | 0.07183 | 0.992 | 188.35 | 1.01 |
| | 15 | 202.0 | 0.07575 | 0.994 | 164.56 | 0.81 |
| | 20 | 480.8 | -0.05911 | 0.994 | 146.65 | 0.31 |

**Table S2.** Folding kinetics table of the previously reported PNIPAM-based and hinge-structured thermo-responsive soft actuators.*

| Active materials | Active layer dimension (LxWxT $mm^3$) | Passive layer | Kinetics control factor | Folding angle (°) | Folding duration (sec) | Folding kinetics (°/sec) | Ref. |
|---|---|---|---|---|---|---|---|
| PNIPAM-NC | 2.4 x 7.0 x 0.6 | PDMS | Phase separation structure | 140-200 | 90-180 | 0.79-2.22 | Our work |
| P(NIPAM-co-NaMAc) | 2.0 x 2.0 x 1.0 | NIPAM | $Fe^{3+}$ crosslinking | 75 | 120 | 0.63 | [1] |
| P(NIPAM-co-SA) | 12.0 x 3 x 0.5 | PP | SA concentration | 160 | 150 | 1.07 | [2] |
| PNIPAM-SWCNT | 3.0 x 5.0 x0.4 | LDPE | SWNT concentration | 90 | 600 | 0.15 | [3] |
| PNIPAM-GO | 25.0 x 5 .0x 1.0 | PNIPAM | Hinge geometry | 160 | 3,600 | 0.04 | [4] |
| P(NIPAM-co-MOEP) | 20.0 x 5.0 x 0.6 | PNIPAM | LiCl crosslinking | 100 | 300 | 0.33 | [5] |
| PNIPAM-MMT | 50.0 x 10.0 x 1.0 | PNIPAM | Gradation | 90 | 30 | 3.0 | [6] |

* NIPAM: N-Isopropylacrylamide, NC: nanoclay(laponite), PDMS: polydimethylsiloxane, NaMAc: sodium methacrylate, SA: stearyl acrylate, PP: polypropylene, LDPE: low-density polyethylene, SWCNT: single-walled carbon nanotube, GO: graphene oxide, MOEP: 2-(methacryloyloxy)ethyl phosphate, and MMT: montmorillonite.

## References


[1] Z. Xu and J. Fu, Programmable and Reversible 3D-/4D-Shape-Morphing Hydrogels with Precisely Defined Ion Coordination, *ACS Applied Materials & Interfaces*, 2020, **12**, 26476-26484.

[2] K. Liu, Y. Zhang, H. Cao, H. Liu, Y. Geng, W. Yuan, J. Zhou, Z. L. Wu, G. Shan, Y. Bao, Q. Zhao, T. Xie and P. Pan, Programmable Reversible Shape Transformation of Hydrogels Based on Transient Structural Anisotropy, *Advanced Materials*, 2020, **32**.

[3] X. Zhang, C. L. Pint, M. H. Lee, B. E. Schubert, A. Jamshidi, K. Takei, H. Ko, A. Gillies, R. Bardhan, J. J. Urban, M. Wu, R. Fearing and A. Javey, Optically- and Thermally-Responsive Programmable Materials Based on Carbon Nanotube-Hydrogel Polymer Composites, *Nano Letters*, 2011, **11**, 3239-3244.

[4] M. Li and J. Bae, Programmable Dual-Responsive Actuation of Single-Hydrogel-Based Bilayer Actuators by Photothermal and Skin Layer Effects with Graphene Oxides, *Advanced Materials Interfaces*, 2023, **10**.

[5] A. B. Baker, D. F. Wass and R. S. Trask, Thermally induced reversible and reprogrammable actuation of tough hydrogels utilising ionoprinting and iron coordination chemistry, *Sensors and Actuators B: Chemical*, 2018, **254**, 519-525.

[6] J. Liu, W. Xu, Z. Kuang, P. Dong, Y. Yao, H. Wu, A. Liu and F. Ye, Gradient porous PNIPAM-based hydrogel actuators with rapid response and flexibly controllable deformation, *Journal of Materials Chemistry C*, 2020, **8**, 12092-12099.